

High-Efficiency All-Dielectric Metasurfaces for Wave-front Tailoring

Mikhail I. Shalaev, Jingbo Sun, Alexander Tsukernik, Apra Pandey, Kirill Nikolskiy, Natalia M. Litchinitser

Department of Electrical Engineering , University at Buffalo, The State University of New York, Buffalo, NY 14260, USA

Toronto Nanofabrication Centre, University of Toronto, Toronto, ON M5S 3G4, Canada

CST of America, Inc., San Mateo, CA 94404, USA

Physics Department, M.V. Lomonosov Moscow State University, Moscow 119991, Russia

KEYWORDS. all-dielectric metasurface, nanoblocks, singular optics, orbital angular momentum, structured light

ABSTRACT. Metasurfaces are two-dimensional optical structures capable of precise manipulation of light propagation, including complete control of the amplitude, phase and polarization of light. As opposed to their conventional, bulk-optics counterparts that rely on long propagation distances, metasurfaces enable beam manipulation within a distance much smaller than light wavelength. A majority of metasurfaces demonstrated to date suffered from low efficiency due to either intrinsic nonradiative losses of metals and orthogonal polarizations coupling or necessity of cascading or working in reflection mode to achieve 360 degrees phase control. Overlapping electric and magnetic dipole resonances in high-index dielectrics enables new opportunities for achieving high efficient, flexible and well-suitable for mass production metasurfaces. Unlike plasmonic, or metal-dielectric based ones, all-dielectric silicon metasurfaces allow to achieve high transmission, do not suffer from Ohmic losses and are compatible with complementary metal–oxide–semiconductor (CMOS) technology. Here we report an experimental demonstration of high-efficiency all-dielectric metasurfaces with full phase control of 360 degrees in transmission mode at telecommunication wavelengths. Silicon-based metasurfaces can be used for fabrication of miniaturized optical components for near-infrared photonics, such as flat lenses, beam deflectors anti-reflection coatings and phase modulators.

Metasurfaces are two-dimensional artificial materials with thicknesses much smaller than incident light wavelength allowing manipulation of light beams and complete control on its phase, amplitude and polarization¹⁻³. Compared to conventional optical elements, relying on long propagation distances, these devices facilitate very strong light-matter interaction allowing abrupt changes of beam parameters. Metasurfaces, unlike its three-dimensional analogues, metamaterials, do not require complicated fabrication techniques and can be fabricated in one lithographical step which makes them very promising for integration on a photonic chip and well suitable for mass production. To date, most work has been focused on metal-dielectric structures, having relatively low efficiency, typically less than 10%, due to necessity of cross-polarized light coupling for full phase coverage and nonradiative Ohmic losses in metals. Some of metasurfaces require cascading in order to achieve 2π phase shift that is not possible using a single layer. Another way of achieving 2π phase shift is to work in the reflection mode only. However, this type of metasurfaces may not be compatible with contemporary semiconductor industry technologies or not well-suitable for mass production.

Recently, it has been shown that both magnetic and electric resonant responses at the same time are possible for high refractive index dielectrics surrounded by low index environment⁴⁻⁷. It is well-known that in case of only one electric or magnetic resonance only π phase shift is possible, while for many useful applications such as lensing, beam deflection, holography and quantum information processing 2π phase shift is required¹. One way to address this problem is to use cross polarized light coupling which is one of the reason of low efficiency of metasurfaces. Another approach is making light to interact with material multiple times by using

of multilayered metasurfaces or operating in reflection mode, complicated fabrication techniques are required for obtaining such kind of devices. In sharp contrast, presence of electric and magnetic resonances simultaneously at the same frequency allows to have 360 degrees phase shift for only single layer structure. It was shown that silicon, having relatively high refractive index at telecommunication wavelength, exhibit both electric and magnetic dipole resonances at the same time⁸⁻¹⁰. Also, it is the most commonly used material in semiconductor industry, which makes it an ideal platform for high-efficient metasurfaces for near-infrared (NIR) wavelength and future integration on optical chip.

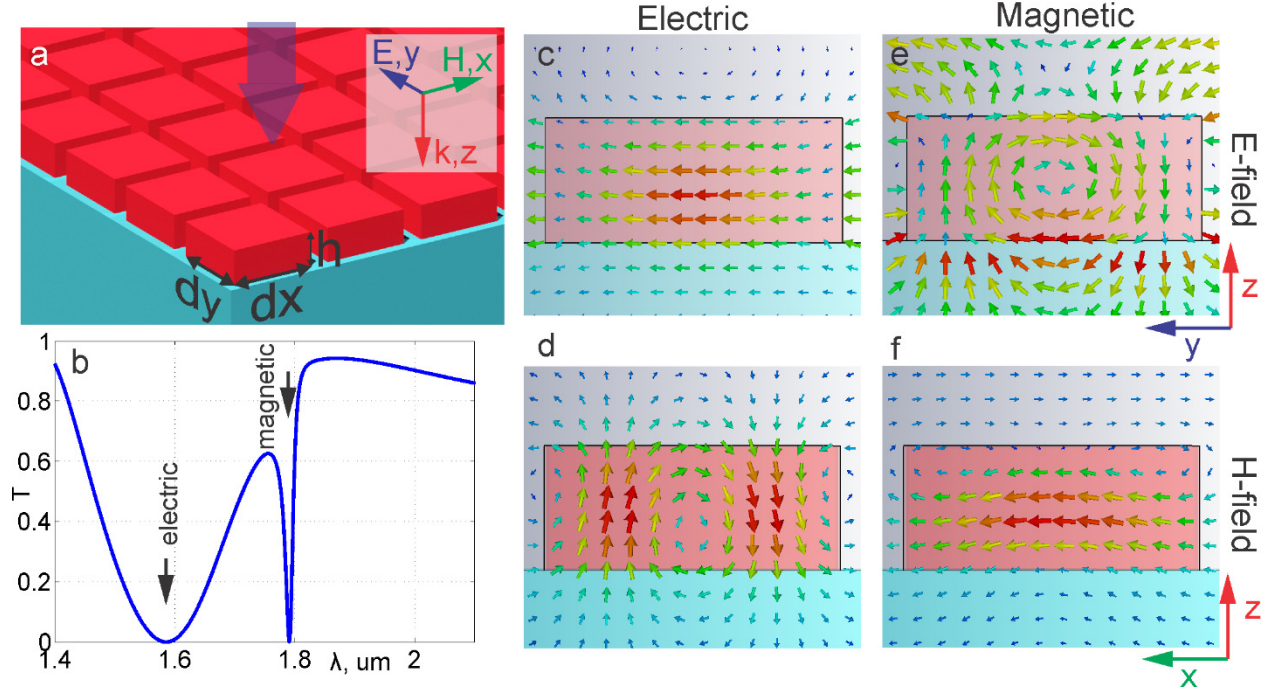


Figure 1. (a) Schematics of silicon nanoblocks metasurface on top of bulk fused silica substrate, blocks height is $h = 270\text{nm}$, dimensions along x and y axes $dx = dy = 650\text{nm}$, lattice constant $a = 800\text{nm}$. (b) Transmission spectrum of metasurfaces shows two dips for electric ($\lambda_e = 1.6\mu\text{m}$) and magnetic ($\lambda_m = 1.8\mu\text{m}$) dipole resonances. (c,d) Electric field enhancement at the center of silicon nanoblocks and vortex-like magnetic field around clearly shows electric dipole resonance while opposite holds for magnetic resonance (e,f) with H -field maximum at the center and twisted E -field around it.

First, we consider light propagation through infinite array of high refractive index polysilicon nanoblocks (refractive index $n = 3.67$) with height $h = 270\text{nm}$ and dimensions $dx = dy = 650\text{nm}$, on top of semi-infinite fused silica substrate (refractive index $n_s = 1.45$), lattice constant $a = 800\text{nm}$, see figure 1a. We used commercially available CST MICROWAVE STUDIO software to perform numerical simulation in frequency domain, incident electromagnetic field assumed to be a plane wave propagating along z axis with electric and magnetic fields polarized along y and x axes correspondingly. Transmission spectrum, shown on figure 1b, clearly shows two dips corresponding to resonant interaction with metasurfaces and, as a result, near unity reflection while the structure assumed to be lossless. Electric and magnetic fields distributions in unit cell cross-section shows electric dipole resonance behavior for wavelength around $\lambda_e = 1.6\mu\text{m}$ with E -field concentrated at the center of nanoblocks and clockwise vortex-like H -field distribution around electric field, see figure 1c,d. Opposite holds for magnetic dipole resonance around $\lambda_m = 1.8\mu\text{m}$ with magnetic field maximum at the center in y - z plane and turbulent electric field around in x - z plane, see figure 1e,f. Here, electric and magnetic resonances are well-separated and can be easily distinguished, but decreasing of blocks size brings resonances to the same region around wavelength of interest, resulting to resonances overlapping

and possibility of impedance matching, near 100% transmission with full phase control. We calculate transmission beam phase depending on silicon blocks size along x and y axes. Two dimensions variation brings additional degrees of freedom and allows designing polarization-dependent metasurfaces while polarization independent design is also possible⁹. Here and for every following design in this letter we assume the wavelength of interest $\lambda_0 = 1.55\mu\text{m}$, lattice constant $a = 800\text{nm}$ and silicon nanoblocks high $h = 270\text{nm}$. Figure 2 shows results of numerical simulation for phase and corresponding transmission coefficients on dx and dy at wavelength of interest, lattice constant and silicon thickness kept the same as ones for figure 1. For metasurfaces functionality we require transmission amplitude to be around the same value, also we constraint dimensions to be no more than 750 nm due to fabrication limitations. Figure 2 can be used for device design for different applications within wide range of block sizes.

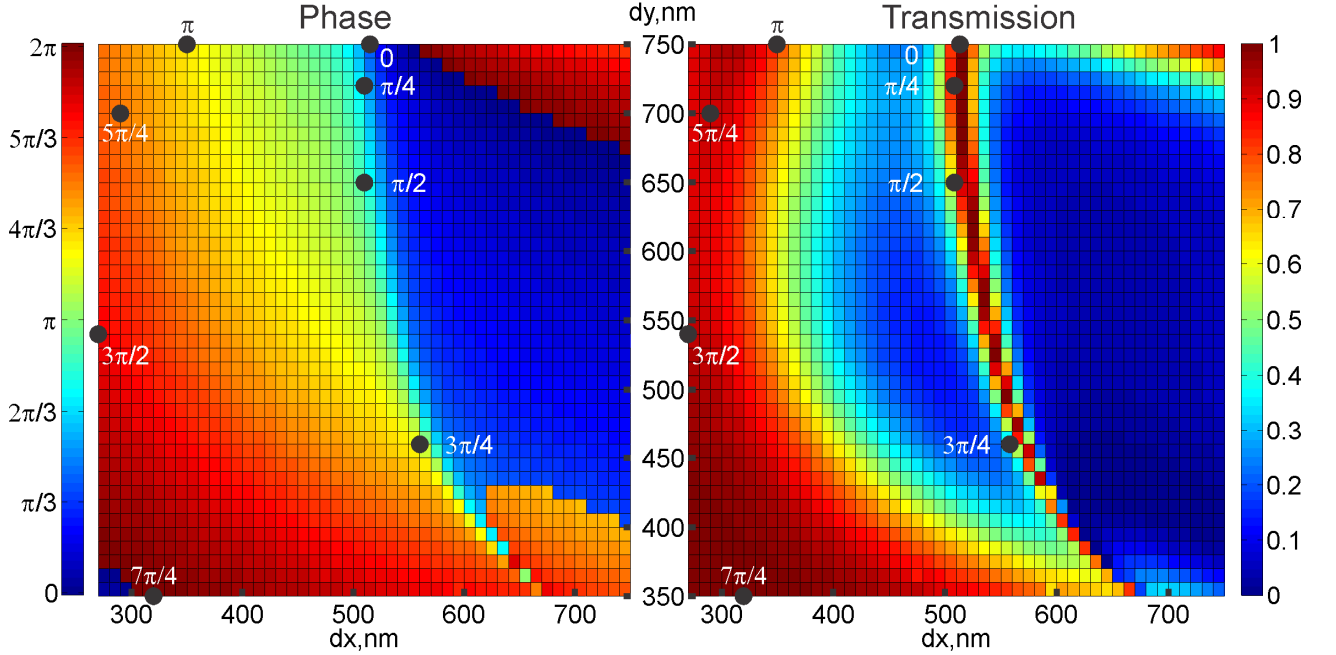


Figure 2. (a) Transmitted light phase variation for nanoblocks on silicon dioxide substrate with lattice constant and (b) normalized transmission intensity dependent on silicon blocks size dx, dy .

We choose eight discrete nanoblocks with $\pi/4$ increments to cover 0-to- 2π phase to provide full phase control of the wavefront. Table 1 shows transmitted light phase for nanoblocks dimensions and corresponding phaseshift.

Table 1. Optimized nanoblocks dimensions.

Phase	0	$\pi/4$	$\pi/2$	$3\pi/4$	π	$5\pi/4$	$3\pi/2$	$7\pi/4$
dx, nm	515	510	510	560	350	290	270	320
dy, nm	750	720	650	460	750	700	540	350

For experimental verification of our numerical simulations we deposited 270nm of silicon with low pressure physical vapor deposition (LPCVD) on top of fused quartz wafers. Fabrication process is shown on figure 3. Then refractive index of deposited silicon was measured to be $n=3.67$ at $1.55\mu\text{m}$ with ellipsometry. We used standard electron beam lithography (EBL) with ZEP520A resist, due to strong charging effect for nonconductive SiO_2 substrate, 20nm thick charge dissipation Cr layer was deposited on e-beam resist. EBL

pattern writing followed by Cr etching with commercially available Cr etchant and development in ZED-N50. Then deep reactive ion etching (DRIE) was performed in C_4F_8 and SF_6 gases followed by resist removing in Remover 1165 at 80C for 1hr and 5 min O_2 plasma for removal of resist residue.

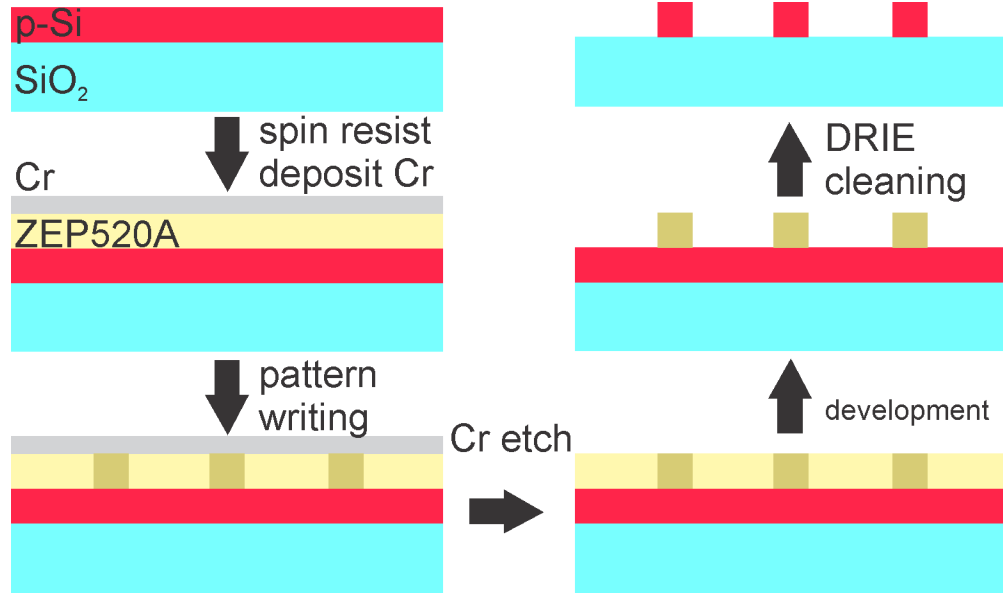


Figure 3. Fabrication process for silicon-based dielectric metasurfaces. We deposit polycrystalline silicon on top of fused silica wafers by low pressure chemical vapor deposition (LPCVD) followed by spin coating of e-beam resist ZEP520A and deposition of 20nm charge dissipation Cr layer. Than pattern was written by electron beam lithography (EBL) and Cr layer was etch by ceric ammonium nitrate-based etchant. Samples were developed in ZED-N50 followed by deep reactive ion etching (DRIE), removal of resist and O_2 plasma cleaning.

We experimentally demonstrated high-efficient full phase manipulation with dielectric metasurfaces at near infrared wavelength with two metasurfaces, one is for optical beam steering and another one - for generating of Laguerre-Gaussian beam from conventional Gaussian light beam. For both cases dramatic changes on light propagation take place within the distance less than $\lambda/5$, opening new possibilities of light control with semiconductor industry compatible materials and easy fabrication procedure. Figure 4a,b shows schematics and scanning electron microscopy (SEM) image for fabricated beam deflection device with $96 \times 96 \mu m$ total size, unit cell is shown in inset, it contains 8 nanoblocks from table 1, where each responsible for phase shift from 0 to 360 with 45 degrees increments. We consider light propagation from isotropic media 1 to media 3 through bulk substrate with metasurfaces on top, see figure 4c inset. Deflection angle for a beam can be calculated with following equation¹¹ $\theta_3 = a \sin \left[(n_1 \sin \theta_1 + \lambda_0 / \Gamma) / n_3 \right]$, where n_{1-3} are refractive indices for medias, θ_1 - incidence angle, λ_0 - free-space wavelength of light, Γ - periodicity of the structure. For our case we consider normal incidence on metasurfaces with structure periodicity $\Gamma = 6.4 \mu m$ on the substrate surrounded by air, refraction angle is $\theta_3 \approx 14^\circ$. We consider plane wave light propagation through infinite array periodic array in x and y directions of silicon nanoblocks depicted. We performed numerical simulations to confirm theoretically calculated refraction angle, figure 3c shows phase of light propagating through the structure Here we assumed substrate thickness to be only $3\lambda_0$ to reduce numerical calculation efforts. As it was predicted refraction angle is around 14 degrees, imperfections and discontinues in light wavefront can be caused by violation of local periodicity in nanostructure that was assumed in phase shift calculations.

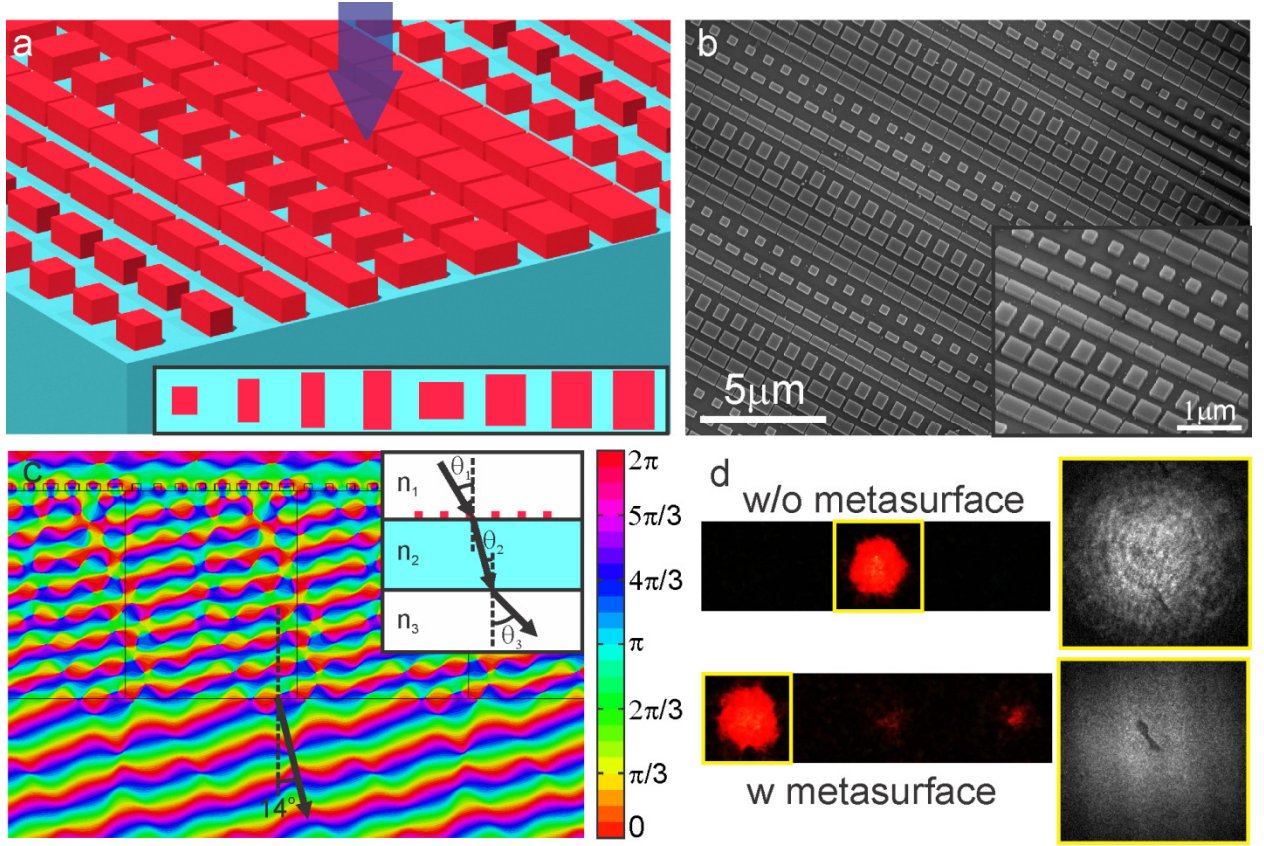


Figure 4. (a) Schematics of beam deflector, with unit cell (shown in inset) contains 8 nanoblocks, each responsible for phase shift from 0 to 360 with 45 degrees increments. (b) Scanning electron microscopy image fabricated metasurfaces with 96x96μm total size, zoomed in picture is shown in inset. (c) Phase of plane wave propagating through the metasurfaces on SiO₂ substrate showing refracted beam angle around 14 degrees. (d) Beam position without (left top) and with (left bottom) metasurface, the most of the beam power is refracted to the left side with deflection angle 13.1° with transmission of ~36%, input and output beams photographs are shown in inset (right).

We used diode laser as light source to perform measurements for beam steering with NIR detector card to determine deflected beam position, schematics of experimental setup is shown in figure 5. The card converts invisible IR signal to visible region, thus deflected beam position was captured by visible light camera. The laser beam was focused by lens to the spot with approximately 45 μm waist. Inset in the left on figure 4d shows results of beams position measurement without (top) and with (bottom) metasurface. As it can be seen the most of the beam power is refracted to the left side of the screen while other diffraction orders can be also seen. Presence of other diffraction orders with much smaller intensity compared to the main beam can be caused by the fact that the unit cell size is comparable to wavelength, not fully satisfying requirement to be much smaller than illuminating light wavelength¹², by imperfections in fabrication process and violation of local periodicity assumed in design. Refraction angle for the main beam is measured to be 13.1° which is close to theoretical and numerical simulations predictions. Insets on the right shows NIR camera images of input and output beams with measured transmission power normalized on input power to be around 36%.

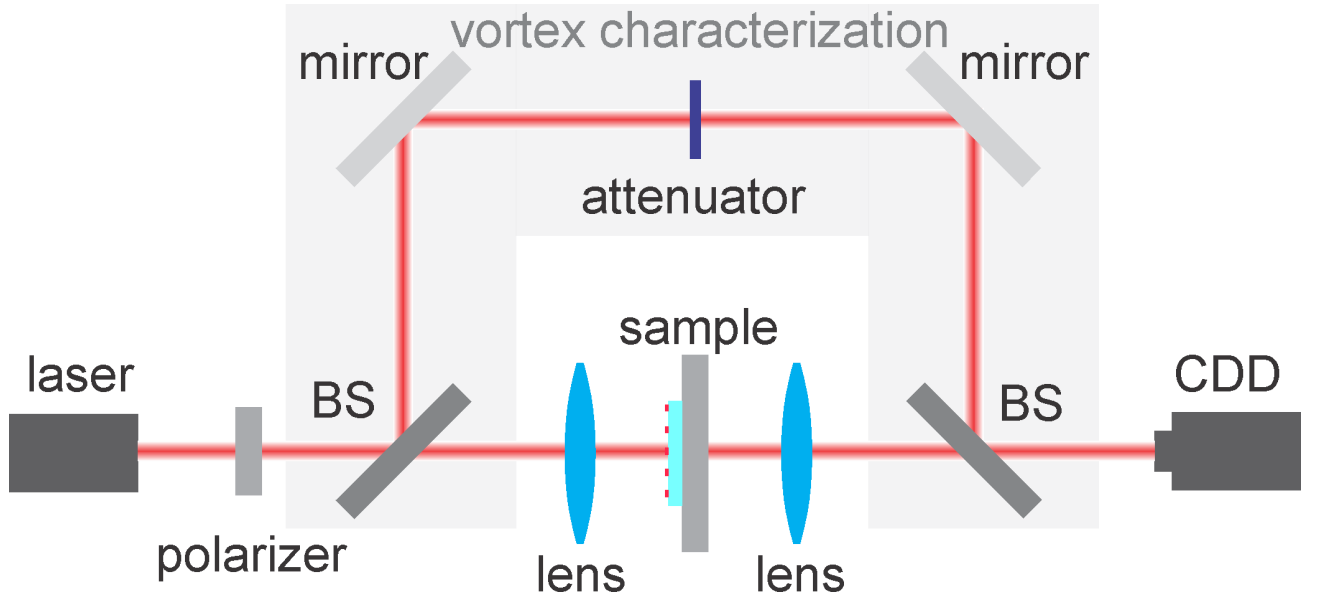


Figure 5. Schematics of experimental setup for measurement of fabricated metasurfaces. Diode NIR laser was used as light source followed by light polarizer, beam was focused to the sample by lens, then collimated and image was captured with CCD camera. Setup for vortex beam interference is shown in gray background, it contains attenuator, two beam splitters and mirrors.

To demonstrate flexibility of designed dielectric nanoblocks for phase control we fabricated light beam convertor to generate Laguerre-Gaussian (LG) beam carrying optical angular momentum from regular Gaussian laser beam. Vortex beams can be used for quantum information processing, high-dimensional communication systems and optical manipulation on nanoscale^{13, 14}. Schematics of fabricated metasurface for twisted beam generation is shown on figure 6a, it contains 8 sectors for particular 0-to- 2π phase shift. LG beam unlike conventional plane wave have donut shape intensity profile and helical wavefront with phase change from 0 to 360 in cross-section. Thus, adding gradual phase shift to Gaussian beam around the beam center result to generating optical vortex [Capasso]. Fabricated beam convertor SEM image is shown on figure 6b, total size is $96 \times 96 \mu\text{m}$. We performed numerical simulations in COMSOL software package for reduced size model with $38.4 \times 38.4 \mu\text{m}$ size and $\sim 25 \mu\text{m}$ incident beam waist on with $2\lambda_0$ thick fused silica substrate to reduce calculation time and memory consumption. Figures 6c,d show transmitted normalized beam intensity and phase at distance of $5\lambda_0$ from metasurface. Phase profile shows gradual phase change around the beam center with donut shape intensity distribution. We believe that imperfections on the beam profile caused by relatively small beam and metasurface sizes with violation of assumption on the same intensity plane wave incident beam assumed before for nanoblocks design at the first part of a letter. Also imperfections can be caused by violation of local periodicity assumed in design. Indeed, experimental results show much more uniform donut-shape intensity profile, see figure 6e. We also perform LG and Gaussian beams interference experiment for both cases of co-propagating (figure 6f) and tilted (figure 6g) beams. As expected images show spiral and fork-like intensity profiles. Transmitted power normalized on input power was measured to be 45%.

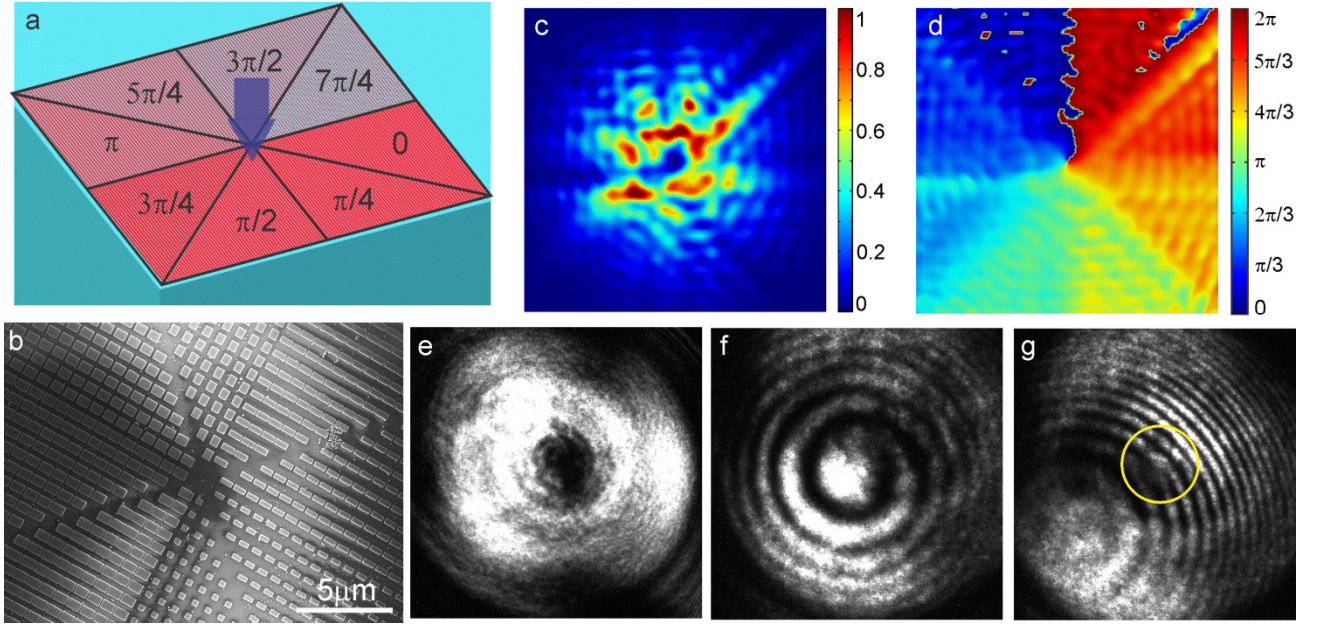


Figure 6. (a) Schematics and (b) scanning electron microscopy image for optical vortex beam converter with 8 sectors with nanoblocks from table 1. Each sector introduce additional 45 degrees phase shift, thus covering 0 to 360 phase. (c,d) Numerically calculated normalized intensity and phase distribution for generated beam with reduced size model at 5 μ m distance from metasurface. (e) Intensity distribution for measured output vortex beam in form of donut shape. (f,g) Laguerre-Gaussian and Gaussian beams interference experiment results showing spiral-shaped and fork-like intensity distribution.

In summary, we have experimentally demonstrated all-dielectric resonant metasurface with full 0-to- 2π phase control at NIR wavelength. We designed and fabricated high-efficient beam deflector and light convertor for generating optical vortex beam, carrying out OAM. Overlapping of magnetic and electric dipole resonance at the same frequency enables 2π phase control with optical impedance matching and, as a result, high efficiency in transmission mode. Fabricated devices made with silicon and, in sharp contrast to plasmonic metasurfaces, are compatible with Complementary metal–oxide–semiconductor (CMOS) technology. Demonstrated metasurfaces have relatively high transmission coefficients of 36% for beam deflector and 45% for LG beam generator. These devices can be fabricated in one lithographical step alleviating the need cascading or working in reflection mode to achieve full phase control. Silicon-based metasurfaces can be used for fabrication of miniaturized high-efficient optical components for NIR photonics, such as flat lenses, beam deflectors, anti-reflection coatings, and phase modulators. Elimination of metals and as a result no Ohmic losses, compared to plasmonic counterparts and does not require cross-polarized field interaction to cover full phase makes them well-suited for integration on optical chip and large-scale production.

1. Zhao, Y.; Liu, X. X.; Alu, A. *J. Opt.* **2014**, 16, (12), 14.
2. Yu, N.; Capasso, F. *Nature Materials* **2014**, 13, (2), 139-150.
3. Lin, D. M.; Fan, P. Y.; Hasman, E.; Brongersma, M. L. *Science* **2014**, 345, (6194), 298-302.
4. Fu, Y. H.; Kuznetsov, A. I.; Miroshnichenko, A. E.; Yu, Y. F.; Luk'yanchuk, B. *Nat. Commun.* **2013**, 4, 6.
5. Person, S.; Jain, M.; Lapin, Z.; Saenz, J. J.; Wicks, G.; Novotny, L. *Nano Lett.* **2013**, 13, (4), 1806-1809.
6. Geffrin, J. M.; Garcia-Camara, B.; Gomez-Medina, R.; Albella, P.; Froufe-Perez, L. S.; Eyraud, C.; Litman, A.; Vaillon, R.; Gonzalez, F.; Nieto-Vesperinas, M.; Saenz, J. J.; Moreno, F. *Nat. Commun.* **2012**, 3, 8.
7. Pfeiffer, C.; Grbic, A. *Phys. Rev. Lett.* **2013**, 110, (19), 5.

8. Decker, M.; Staude, I.; Falkner, M.; Dominguez, J.; Neshev, D. N.; Brener, I.; Pertsch, T.; Kivshar, Y. S. *Advanced Optical Materials* **2015**, 3, (6).
9. Cheng, J. R.; Ansari-Oghol-Beig, D.; Mosallaei, H. *Opt. Lett.* **2014**, 39, (21), 6285-6288.
10. Staude, I.; Miroshnichenko, A. E.; Decker, M.; Fofang, N. T.; Liu, S.; Gonzales, E.; Dominguez, J.; Luk, T. S.; Neshev, D. N.; Brener, I.; Kivshar, Y. *ACS Nano* **2013**, 7, (9), 7824-7832.
11. Yu, N. F.; Genevet, P.; Kats, M. A.; Aieta, F.; Tetienne, J. P.; Capasso, F.; Gaburro, Z. *Science* **2011**, 334, (6054), 333-337.
12. Larouche, S.; Smith, D. R. *Opt. Lett.* **2012**, 37, (12), 2391-2393.
13. Wang, J.; Yang, J. Y.; Fazal, I. M.; Ahmed, N.; Yan, Y.; Huang, H.; Ren, Y. X.; Yue, Y.; Dolinar, S.; Tur, M.; Willner, A. E. *Nat. Photonics* **2012**, 6, (7), 488-496.
14. Willner, A. E.; Wang, J.; Huang, H. *Science* **2012**, 337, (6095), 655-656.